ELSEVIER

Coordination Chemistry Reviews
216–217 (2001) 31–43

COORDINATION CHEMISTRY REVIEWS

www.elsevier.com/locate/ccr

Photochemistry and electronic spectroscopy of the $Ru(SnPh_3)_2(CO)_2(\alpha$-diimine) complexes: an ab initio investigation of the model system $Ru(SnH_3)_2(CO)_2$(Me-DAB) (DAB = 1,4-diaza-1,3-butadiene)

Mohamed Turki, Chantal Daniel *

Laboratoire de Chimie Quantique UMR 7551 CNRS/Université Louis Pasteur Institut LeBel, 4 Rue Blaise Pascal, 67000 Strasbourg, France

Received 8 August 2000; received in revised form 14 February 2001; accepted 2 March 2001

Contents

Abstract

The low-lying excited states and associated potential energy curves of $Ru(SnH_3)_2(CO)_2$-(Me-DAB), model system for the $Ru(SnPh_3)_2(CO)_2(\alpha$-diimine) complexes, have been calculated at the complete active space SCF (CASSCF) and complete active space perturbation theory second-order (CASPT2) levels. The experimental spectrum has been assigned without

* Corresponding author. Tel.: +33-388-416076; fax: +33-388-612085.
E-mail address: daniel@quantif.u-strasbg.fr (C. Daniel).

0010-8545/01/$ - see front matter
PII: S0010-8545(01)00360-5

any ambiguity. A mechanism has been proposed for the Ru–Sn bond homolysis, process occuring after irradiation of the title complex in the visible. The presence of a low-lying ^{3}SBLCT state with a pre-dissociative character is responsible for this primary reaction and for the long-lifetime emission observed with a low quantum yield.

Keywords: Photochemistry; Electronic spectroscopy; Model system

1. Introduction

A new class of transition metal carbonyl–diimine complexes $Ru(E)(E')(CO)_2$(α-diimine) (E,E′ = halide, alkyl, benzyl, metal fragment) have been studied intensively in the past five years for their remarkable photochemical, photophysical and electrochemical properties [1–12]. These molecules have a great potential as luminophores, photosensitisers and initiators of radicals and represent a challenge to the understanding of excited state dynamics. Careful spectroscopic investigations supported by an analysis based on DFT calculations have put in evidence an unusually extensive and flexible electronic delocalisation over four centres, namely the central metal atom, the α-diimine π acceptor ligand and the axial ligands E and E′ [5]. In the presence of a covalently bound axial ligand in the sphere of coordination, a low-lying σπ* excited state that involves excitation from the metal-ligand bounding orbital to the π* of the α-diimine ligand is responsible for a variety of photochemical responses, depending on the nature of the axial ligands E and E′ [12]. In the $Ru(E)(E')(CO)_2$(*i*-Pr-DAB) complexes where both E and E′ are coordinated through a Group 14 metal atom (Sn, Ge, Pb) a rather strong interaction between the Ru(E)(E′) fragment and the π* α-diimine leads to an extensive electron delocalisation and an unusual long-lived excited state ^{3}σπ* detected by an intense and long-lived emission (264 μs) at 670 nm [5,7,8]. In THF, the absorption spectrum is characterised by an intense band at 511 nm (19 570 cm^{-1}) attributed to the ^{1}σπ* state so-called sigma-bond-to-ligand-charge-transfer (SBLCT) and a shoulder at 450 nm (22 200 cm^{-1}) assigned to a low-lying metal-to-ligand-charge-transfer (MLCT) excited state [7]. A new band is formed in the near-UV around 330 nm. After irradiation into the intense band between 500 and 550 nm, homolytic splitting of the Ru–Sn bond is observed [6]:

$$Ru(ShPh_3)_2(CO)_2(i\text{-Pr–DAB}) \xrightarrow{h\nu} {}^{\bullet}SnPh_3 + {}^{\bullet}Ru(SnPh_3)(CO)_2(i\text{-Pr–DAB}) \qquad (1)$$

with a quantum yield ϕ_{Ru-Sn} of around 0.23 at room temperature. This primary reaction is rather slow (μs time-scale), thermally activated but wavelength independent.

On the basis of the experimental data and DFT calculations, the following qualitative mechanism has been proposed [12]: the molecule becomes trapped in the potential well of the bound SBLCT (^{3}σπ*) state, which presents a pre-dissociative character (with an activation energy estimated to 1460 cm^{-1}) due to its avoided crossing with a higher dissociative state leading to the diradical primary products.

In order to understand the dual behaviour of $Ru(SnPh_3)_2(CO)_2$(*i*-Pr-DAB), namely a long-lived emission together with a rather slow but efficient dissociative process, we have undertaken a detailed theoretical study of the model system $Ru(SnH_3)_2(CO)_2$(Me-DAB) based on complete active space SCF (CASSCF) calculations supplemented by multireference contracted configuration interaction (MR-CCI) and complete active space perturbation theory second-order (CASPT2) treatments. The present contribution will be devoted to the visible part of the absorption spectrum and to the photoreactivity of the low-lying singlet and triplet excited states.

2. Computational details

Ab initio calculations have been performed on the DFT (B3LYP) optimised structure for the $^1A_1$ electronic ground state in C_{2v} symmetry [13] (Fig. 1).

The electronic ground state configuration corresponds to the following: $(\sigma 1_{Sn-Ru-Sn})^2$ $(4d_{xy})^2(4_{dy2-z2})^2(4d_{xy})^2(\sigma 2_{Sn-Ru-Sn})^2$ where $\sigma 1$ of symmetry a_1 and $\sigma 2$ of symmetry b_1 represent the bonding orbitals between the sp(Sn) orbitals of the SnH_3 ligands with the $4d_{z2}$(Ru) and $4p_z$(Ru) orbitals, respectively (Scheme 1).

Ten electrons have been correlated in 12 active orbitals in the CASSCF calculations.These active orbitals correspond to the 4d of the metal centre, the $\sigma 1$ and $\sigma 2$ bonding orbitals and their antibonding counterparts $\sigma 1^*$ and $\sigma 2^*$, the low-lying π^*_{Me-DAB} and four low-lying π^*_{CO} orbitals. Averaged CASSCF calculations (over five roots in C_{2v} and eight roots in C_s) have been performed for a given spin and symmetry in order to treat in a balanced way the various electronic states characterising this molecule. The CASSCF wave functions have been used as references in subsequent MR-CCI and CASPT2 calculations using the level shift corrected perturbation method [14] with a value of 0.25. The stability of the perturbational treatment has been evaluated by performing several calculations

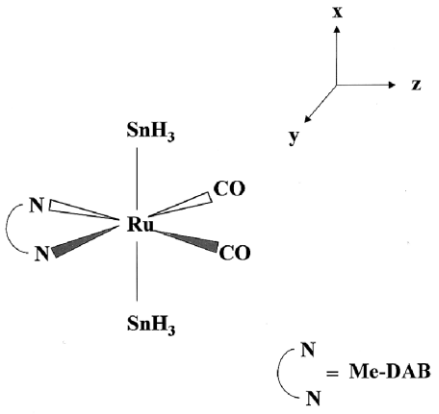

Fig. 1. Idealised structure of $Ru(SnH_3)_2(CO)_2$(Me-DAB).

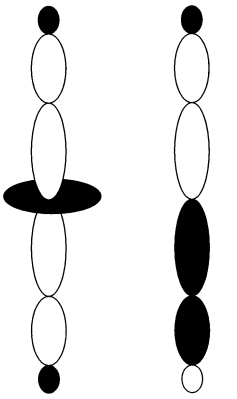

Scheme 1. Symmetric and antisymmetric Ru–Sn bonding orbitals in $[Ru(SnH_3)_2(CO)_2(Me–DAB)]$.

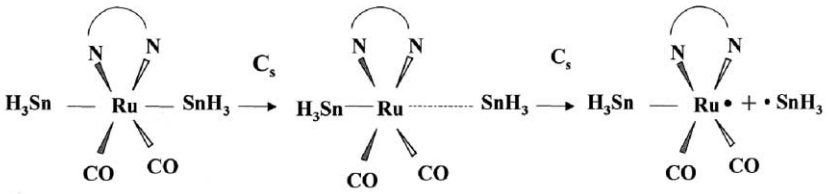

Scheme 2. Homolytic rupture of the Ru–Sn bond in $[Ru(SnH_3)_2(CO)_2(Me–DAB)]$ under the C_s symmetry constraint.

varying the level-shift values. Ten electrons have been correlated in the CI calculations to the whole virtual space, including single and double excitations on a multireference scheme. All the configurations appearing with a coefficient larger than 0.08 have been added as references. Relativistic effective core potentials have been used with the following associated valence basis sets: for the Ru atom ($Z = 16.0$) an (8s, 7p, 6d) set contracted to [6s, 5p, 3d] [15], for the Sn atoms ($Z = 4.0$) a (4s, 4p) set contracted to [2s, 2p] [16], for the second row atoms C ($Z = 4.0$) a (4s, 4p) set contracted to [2s, 2p] and O ($Z = 6.0$) a (4, 5) set contracted to [2s, 3p] [16] and for the H atoms a (7s) contracted to [2s] [17]. Spin–orbit coupling effects, which should be very important in this molecule, are not included in the present work and will be the subject of further study.

The deformation of the molecule when going from the $^1A_1$ electronic ground state to the absorbing state ^{1}SBLCT ($\sigma^2 \rightarrow \pi^*_{Me–DAB}$) and to the corresponding ^{3}SBLCT (supposed to be the long-lived state) has been investigated by gradient–CASSCF geometry optimisations under the C_{2v} symmetry constraint. The potential energy curves connecting the $Ru(SnH_3)_2(CO)_2$(Me-DAB) low-lying excited states to

those of the Ru–SnH_3 bond homolysis primary products have been calculated under the C_s symmetry constraint varying one Ru–SnH_3 bond elongation (Scheme 2), the other degrees of freedom being frozen. This is justified by the small Stokes shifts measured for the $Ru(SnPh_3)_2(CO)_2$(*i*-Pr–DAB) complex associated with a minor distortion of the SBLCT state. The ab initio calculations were carried out with the Molcas 4.1 system of programs [18].

3. Results and discussion

3.1. Electronic spectroscopy

The low-lying excited states contributed to the visible/near-UV absorption spectrum of $Ru(SnH_3)_2(CO)_2$(Me-DAB) and the associated triplet states, calculated at the CASSCF/CASPT2 level, are reported in Table 1. The $^1A_1 \rightarrow {}^1A_1$, $^1A_1 \rightarrow {}^1B_1$ and $^1A_1 \rightarrow {}^1B_2$ allowed transitions have been calculated together with their oscillator strengths.

Only the low-lying states below 35 000 cm^{-1} are reported here, the whole electronic spectrum (until the far-UV region) being the subject of another study combining CASSCF/CASPT2 and TD-DFT calculations [19]. The CASSCF excitation energies are only qualitative and overestimated by nearly 1.0 eV and will not be discussed here. The dynamical electronic correlation added at the perturbational level of theory (CASPT2) will correct these well-known effects.

The lowest excited state b^1A_1 calculated at 21 060 cm^{-1} with an oscillator strength $f = 0.173$ is mainly of SBLCT character ($\sigma 2_{\text{Sn–Ru–Sn}} \rightarrow \pi^*_{\text{Me–DAB}}$) with a contribution of MLCT ($4d_{xz} \rightarrow \pi^*_{\text{Me–DAB}}$). This state can be attributed without any ambiguity to the first intense band observed at 511 nm (19 570 cm^{-1}) in THF and characterised as an SBLCT transition. The shoulder at 450 nm (22 220 cm^{-1}) can be assigned to the $a^1A_1 \rightarrow a^1B_2$ transition corresponding to a pure MLCT state ($4d_{xz} \rightarrow \pi^*_{\text{Me–DAB}}$) calculated at 24 440 cm^{-1} with a very low oscillator strength ($f = 0.005$). A third singlet state mainly of MLCT character ($4d_{xz} \rightarrow \pi^*_{\text{Me–DAB}}$) with a contribution of SBLCT character ($\sigma 2_{\text{Sn–Ru–Sn}} \rightarrow \pi^*_{\text{Me–DAB}}$) and calculated at 29 020 cm^{-1} with an oscillator strength $f = 0.133$ should correspond to the absorption in the UV region starting at 330 nm (30 303 cm^{-1}). The next two $a^1A_1 \rightarrow {}^1B_1$ transitions calculated at 32 830 and 33 810 cm^{-1} are nearly degenerate and correspond to mixed MLCT ($4d_{xz} \rightarrow \pi^*_{\text{Me–DAB}}$) and SBLCT ($\sigma 1_{\text{Sn–Ru–Sn}} \rightarrow \pi^*_{\text{Me–DAB}}$) states. Although the low-lying singlet states are not completely pure, the corresponding triplet states do not show any significant SBLCT/MLCT mixed character. The lowest triplet state calculated at 15 640 cm^{-1} is purely SBLCT and corresponds to the ($\sigma 2_{\text{Sn–Ru–Sn}} \rightarrow \pi^*_{\text{Me–DAB}}$) excitation, whereas the two next triplet states are purely MLCT states in the Franck–Condon region. The a^3B_2 state calculated at 22 930 cm^{-1} corresponds to the ($4d_{xz} \rightarrow \pi^*_{\text{Me–DAB}}$) excitation and the b^3A_1 state calculated at 27 140 cm^{-1} corresponds to the ($4d_{xz} \rightarrow \pi^*_{\text{Me–DAB}}$) excitation. The $^3B_1$ states calculated around 32 000 cm^{-1} show the same SBLCT/MLCT mixed character as the corresponding singlet states.

Table 1
CASSCF/CASPT2 and CASSCF/MR-CCI excitation energies (in cm^{-1}) and oscillator strengths of the low-lying electronic states of $Ru(CO)_2(SnH_3)_2$(Me-DAB)[a]

State	One-electron excitations in the principal configuration	CASSCF excitation energy	CASPT2 excitation energy [a]	f	MR-CCI [b]
$a^1A_1 \rightarrow b^1A_1$	$(\sigma 2_{Sn-Ru-Sn} \rightarrow \pi^*_{Me-DAB})$	27 080	21 060	0.173	27 540
SBLCT/MLCT	$(4d_{xz} \rightarrow \pi^*_{Me-DAB})$				(26 470)
$a^1A_1 \rightarrow a^1B_2$	$(4d_{xz} \rightarrow \pi^*_{Me-DAB})$	32 540	24 440	0.005	
MLCT					
$a^1A_1 \rightarrow c^1A_1$	$(4d_{xz} \rightarrow \pi^*_{Me-DAB})$	35 230	29 020	0.133	34 830
MLCT/SBLCT	$(\sigma 2_{Sn-Ru-Sn} \rightarrow \pi^*_{Me-DAB})$				(34 580)
$a^1A_1 \rightarrow a^1B_1$	$(4d_{xz} \rightarrow \pi^*_{Me-DAB})$	37 180	32 830	0.003	36 140
MLCT/SBLCT	$(\sigma 1_{Sn-Ru-Sn} \rightarrow \pi^*_{Me-DAB})$				(36 280)
$a^1A_1 \rightarrow b^1B_1$	$(\sigma 1_{Sn-Ru-Sn} \rightarrow \pi^*_{Me-DAB})$	36 580	33 810	0.018	37 160
SBLCT/MLCT	$(4d_{xz} \rightarrow \pi^*_{Me-DAB})$				(36 820)
$a^1A_1 \rightarrow a^3A_1$	$(\sigma 2_{Sn-Ru-Sn} \rightarrow \pi^*_{Me-DAB})$	15 280	15 640		16 540
SBLCT					(16 350)
$a^1A_1 \rightarrow a^3B_2$	$(4d_{xz} \rightarrow \pi^*_{Me-DAB})$	30 800	22 930		
MLCT			–		
$a^1A_1 \rightarrow b^3A_1$	$(4d_{xz} \rightarrow \pi^*_{Me-DAB})$	31 540	27 140		30 920
MLCT					(30 490)
$a^1A_1 \rightarrow a^3B_1$	$(4d_{xz} \rightarrow \pi^*_{Me-DAB})$	35 450	32 540		35 000
MLCT/SBLCT	$(\sigma 2_{Sn-Ru-Sn} \rightarrow \pi^*_{Me-DAB})$				(34 180)
$a^1A_1 \rightarrow b^3B_1$	$(\sigma 1_{Sn-Ru-Sn} \rightarrow \pi^*_{Me-DAB})$	34 480	32 540		35 200
SBLCT/MLCT	$(4d_{xz} \rightarrow \pi^*_{Me-DAB})$				(34 880)

[a] With a level-shift correction of 0.25.
[b] Values obtained with the ACPF correction are given in parentheses.

Surprisingly, the MR-CCI treatment does not improve the excitation energies with respect to the CASSCF values. Clearly, a large number of electrons (more than the ten electrons correlated either in the CASSCF or in the MR-CCI approach) have to be correlated in order to take into account the important electronic delocalisation effects which characterise the various excited states. This effect is even more dramatic in the case of the low-lying singlet states which have mixed characters. For this reason, the MR-CCI method will not be used for a subsequent building of the potential energy curves. A perturbative treatment seems to be more appropriate (CASPT2).

In order to follow the geometrical deformations in the low-lying ^{1,3}SBLCT exited states, gradient–CASSCF geometry optimisations have been performed under the C_{2v} symmetry constraint. The resulting optimised structures are depicted in Fig. 2.

The DFT (B3LYP) optimised geometry of the $^1A_1$ electronic ground state [13] as well as the experimental structure [7] are given as references. In agreement with the small observed Stokes shift, the distortions which characterise the low-lying SBLCT states of the $Ru(SnH_3)_2(CO)_2$(Me-DAB) complex are not significant. The main deformation concerns the Ru–Sn bond, which is elongated when going from the electronic ground state to the SBLCT states. In order to infer the dissociative character of these states, preliminary 2D potentials have been calculated under the C_{2v} symmetry constraint as a function of the symmetric elongations of the two Ru–Sn bonds [20]. The bound shape of these potentials indicates clearly that a synchronous symmetric dissociation of both SnH_3 fragments is unlikely. In contrast, the mechanism should go through the homolytic rupture of one specific Ru–Sn bond breaking the C_{2v} symmetry (Scheme 2).

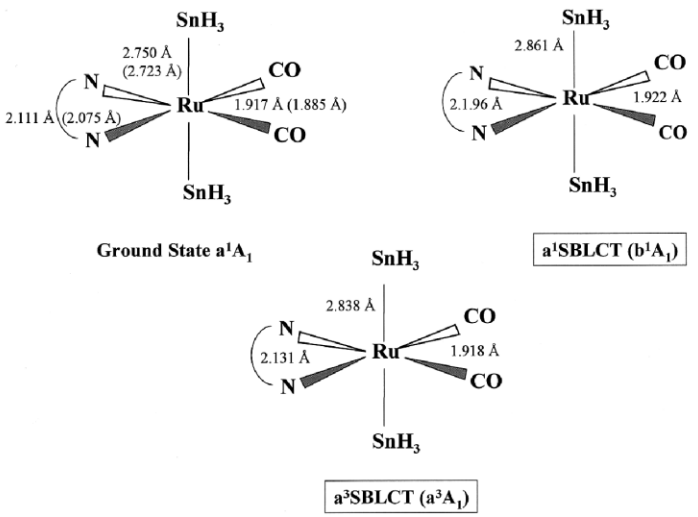

Fig. 2. Gradient–CASSCF optimised bond lengths of $Ru(SnH_3)_2(CO)_2$(Me-DAB) in the electronic ground state a^1A_1, a^1SBLCT and a^3SBLCT states. The DFT values are reported in parentheses for the electronic ground state.

3.2. Homolysis of the Ru–Sn bond

The CASSCF potential energy curves calculated under the C_s symmetry constraint as a function of the $q_a = [Ru–Sn]$ bond elongation and associated to the electronic ground state (a^1A_1 or a^1A') and the low-lying $a^{1,3}$SBLCT (b^1A_1 or b^1A' and a^3A_1 or a^3A') and a^3MLCT (b^3A_1 or b^3A') of $Ru(SNH_3)_2(CO)_2$(Me-DAB) are depicted in Fig. 3. The labels reported in Fig. 3 correspond to the main electronic stucture around the equilibrium geometry. Obviously, the character of the potential energy curves may evolve as a function of the Ru–Sn bond elongation.

The corresponding CASSCF energies are reported in Table 2. The CASSCF excitation energies deduced from the results reported in Table 2 for $q_a = [Ru–Sn] =$ 2.72 Å (equilibrium geometry) differ slightly from those reported in Table 1 because of an artefact of the calculations performed under the C_s symmetry constraint. The b^1A_1 state is calculated at 27 360 cm^{-1} (vs 27 080 cm^{-1} under the C_{2v} symmetry constraint) and the low-lying a^3A_1 and b^3A_1 at 14 840 cm^{-1} (vs 15 280 cm^{-1}) and 30 030 cm^{-1} (vs 31 540 cm^{-1}), respectively. The potential energy curves represented in Fig. 3 are only qualitative, the important dynamical correlation effects having their origin in the multiple excitations of the inactive CASSCF electrons being included in a more refined treatment based on the perturbation theory (CASPT2, see next paragraph).

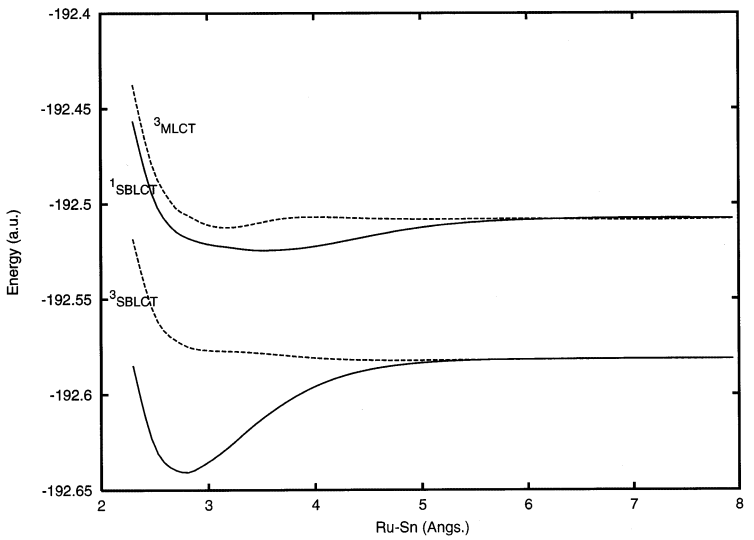

Fig. 3. Adiabatic CASSCF potential energy curves associated to the a^1A_1 (GS) electronic ground state and to the low-lying $^{1,3}A_1$ (a^1SBLCT, a^3SBLCT) and $^3B_1$ (a^3MLCT) excited states of $Ru(SnH_3)_2(CO)_2$(Me-DAB) calculated under the C_s symmetry constraint as a function of the $q_a =$ [Ru–Sn] bond elongation.

Table 2
CASSCF and CASPT2 (in italic) energies (in a.u. and relative to −192 and −193, respectively) of the electronic ground state and the a^3SBLCT, b^1SBLCT and a^3MLCT states of $Ru(CO)_2(SnH_3)_2$(Me-DAB) as a function of the q_a = [Ru–Sn] bond elongation in Å. The correspondence in C_{2v} at the equilibrium geometry (q_a = 2.72 Å) is given in parenthesis

	q_a = [Ru–Sn]																	
	2.3	2.5	2.6	2.72	2.8	2.9	3.0	3.2	3.4	3.6	3.8	4.0	4.2	4.5	5.0	6.0	7.0	50.0
$a^1A'(a^1A_1)$	0.58493	0.62741	0.63617	0.64006	0.64077	0.63865	0.63531	0.62707	0.61736	0.60886	0.60166	0.59590	0.59155	0.58721	0.58361	0.58146	0.58106	0.58143
	0.90585	*0.94235*	*0.94966*	*0.95226*	*0.95130*	*0.94819*	*0.94337*	*0.93153*	*0.91741*	*0.90562*	*0.89544*	*0.88702*	*0.88036*	*0.87303*	*0.86613*	*0.86123*	*0.86008*	*0.85884*
$a^3A'(a^3A_1)$	0.51851	0.55828	0.56742	0.57245	0.57484	0.57631	0.57694	0.57741	0.57804	0.57901	0.58004	0.58093	0.58159	0.58215	0.58231	0.58184	0.58160	0.58139
a^3SBLCT	*0.83259*	*086909*	*087649*	*087933*	*0.87878.*	*087756*	*0.87300*	*0.86896*	*0.86598*	*0.86424*	*0.86330*	*0.86279*	*0.86235*	*0.86153*	*0.85997*	*0.85758*	*0.85651*	*0.85564*
b^1A' (b^1A_1)	0.45658	0.49825	0.50845	0.51537	0.51771	0.51977	0.52123	0.52281	0.52426	0.52444	0.52381	0.52244	0.52053	0.51726	0.51258	0.50851	0.50765	0.50781
b^1SBLCT/ ^{1}MLCT	*0.80601*	*0.84164*	*0.84977*	*0.85392*	*0.85434*	*0.85334*	*0.85076*	*0.84380*	*0.83586*	*0.83127*	*0.82784*	*0.82486*	*0.82198*	*0.81752*	*0.81081*	*0.80387*	*0.80211*	*0.80071*
$b^3A'(b^3A_1)$	0.43754	0.48320	0.49435	0.50323	0.50567	0.50877	0.51106	0.51245	0.51094	0.50867	0.50727	0.50697	0.50722	0.50777	0.50822	0.50802	0.50780	0.50751
a^3MLCT	*0.77029*	*0.81277*	*0.82227*	*0.82778*	*0.82649*	*0.82549*	*0.82100*	*0.81706*	*0.81268*	*0.80896*	*0.80646*	*0.80486*	*0.80369*	*0.80232*	*0.80062*	*0.79824*	*0.79736*	*0.79656*

The lowest potential energy curves are described entirely by two main electronic configurations corresponding to the ($\sigma 2_{\text{Sn–Ru–Sn}} \rightarrow \pi^*_{\text{Me–DAB}}$) and ($4d_{xz} \rightarrow \pi^*_{\text{Me–DAB}}$) excitations, the mixing of which varies smoothly as a function of the Ru–Sn bond elongation in the low-lying singlet excited state. The lowest triplet states remain nearly pure along the dissociation pathway. Around 3.4 Å, the $\pi^*_{\text{Me-DAB}}$ orbital interacts with the $\sigma 1^*$ orbital and at 50.0 Å, the lowest triplet state (a^3A'), which becomes degenerate with the a^1A' state (formation of the diradical with $E = -192.58143$ a.u.), is described by the ($\sigma 2 \rightarrow \pi^*_{\text{Me–DAB}}/\sigma 1^*$) excitation, the $\sigma 2$ and $\pi^*_{\text{Me-DAB}}/\sigma 1^*$ orbitals being localised on the $^{\bullet}SnH_3$ and $^{\bullet}Ru(SnH_3)(CO)_2$(Me-DAB) fragments, respectively. The ^{3}SBLCT state keeps its main character (78%) from the equilibrium geometry ($d_{\text{Ru–Sn}} = 2.72$ Å) to the homolysis primary products (71%). The ^{3}MLCT state is nearly pure at equilibrium (76%) and gains some sigma-bond–sigma-bond charge transfer (SBSBCT) character (18%) around 3.4 Å. This contribution, corresponding to a $\sigma 2 \rightarrow \sigma 1^*/\pi^*_{\text{Me–DAB}}$ excitation, reaches 33% at dissociation. According to the shape of the potentials depicted in Fig. 3, the absorbing a^1SBLCT (b^1A') state is bound with respect to the Ru–Sn bond elongation and should not be responsible for the observed reactivity. The lowest a^3SBLCT state seems to be nearly dissociative with a shallow minimum around the equilibrium geometry and an inflexion around 3.6 Å. This state correlates with the primary products of reaction (1) in their ground states $a^{1,3}A'$ but does not show any distinct pre-dissociative character in contrast to the predictions based on spectroscopical investigations [12]. Regarding the large energy gap between this state and the absorbing state, the a^1SBLCT $\rightarrow a^3$SBLCT intersystem should occur in a rather long time-scale (beyond the ps) and should not be very efficient. Indeed, we have shown recently [21,22] that intersystem crossings in transition metal complexes are relatively fast (ps time-scale) and efficient in situations of critical geometries (singlet/triplet crossing) close to the Franck–Condon region.

The corresponding CASPT2 potential energy curves are depicted in Fig. 4 and differ significantly from the CASSCF potentials. The corresponding CASPT2 energies are reported in Table 2.

An increase of the binding energy by 0.03 a.u. is observed when using a highly correlated method. This reflects the importance of the dynamical correlation effects around the Franck–Condon region where the electronic relaxation is crucial. This is illustrated by the dependence on the Ru–Sn bond elongation of the CASPT2 correction to the zero-order CASSCF energies. The differences in these corrections may reach 6000–7000 cm^{-1} between the equilibrium geometry ($d_{\text{Ru–Sn}} = 2.72$ Å) and the dissociation ($d_{\text{Ru–Sn}} = 50.0$ Å). The CASPT2 correction may also vary from one electronic state to the next one, depending on its spin and character. For instance, at the equilibrium geometry, the difference between the CASPT2 corrections rises to 7000 cm^{-1} with an important lowering of the ^{1}SBLCT as compared to the ^{3}SBLCT state. This can be explained by the better description of the triplet states at the zero-order and by the presence of the MLCT contribution involving the metal atom in the singlet state which does not exist in the triplet state and which may be responsible for large dynamical correlation effects. Similarly, the ^{3}MLCT

state delocalised over the metal centre and the DAB ligand is more stabilised by the perturbative treatment (by 4000 cm^{-1}) than the ^{3}SBLCT state. The near degeneracy of the ^{1}SBLCT and ^{3}MLCT states obtained at the CASSCF level around the equilibrium distance ($d_{Ru-Sn} = 2.72$ Å) is raised at the CASPT2 level. The main consequence of these electronic correlation effects is the change in the shape of the ^{3}SBLCT potential energy curve which appears to be pre-dissociative at the CASPT2 level of theory with an energy barrier of 2300 cm^{-1} slightly oversestimated with respect to the one derived from temperature-dependence experiments.

On the basis of the lowest excited states which have been assigned without any ambiguity and of the shape of the associated potential energy curves, the following mechanism can be proposed to account for the experimental observations, namely a long-lived excited state and a rather slow but thermally activated and wavelength-independent homolysis of the Ru–Sn bond occuring from a single triplet excited state:

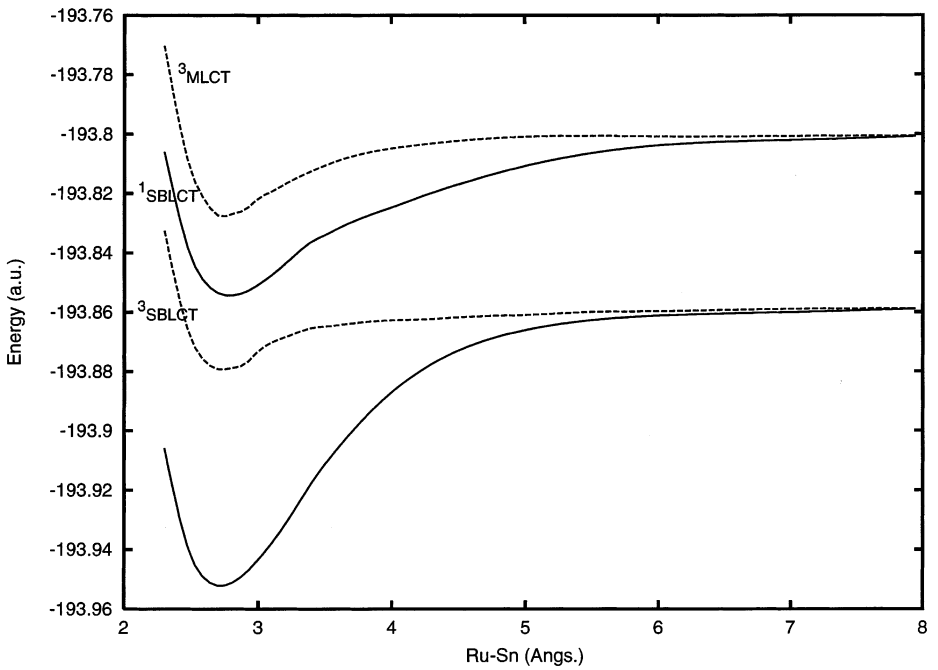

Fig. 4. Adiabatic CASPT2 potential energy curves associated to the a^1A_1 (GS) electronic ground state and to the low-lying $^{1,3}A_1$ (a^1SBLCT, a^3SBLCT) and $^3B_1$ (a^3MLCT) excited states of $Ru(SnH_3)_2(CO)_2$(Me-DAB) calculated under the C_s symmetry constraint as a function of the q_a = [Ru–Sn] bond elongation.

1. After absorption to the a^{1}SBLCT at 500 nm and intramolecular vibrational relaxation (IVR) the system gets trapped in the potential well of the ^{1}SBLCT state.
2. From there, slow intersystem crossing of low efficiency to the ^{3}SBLCT state may occur, followed by two different deactivation processes, depending on the experimental conditions (temperature).
3. The ^{3}SBLCT state may either lead to the formation of the $^{\bullet}Ru(SnH_3)(CO)_2$(Me-DAB) and $^{\bullet}SnH_3$ primary products in their ground states or to a long-lifetime emission to the electronic ground state of $Ru(SnH_3)_2(CO)_2$(Me-DAB).

4. Concluding remarks

On the basis of accurate ab initio calculations of the low-lying excited states of $Ru(SnH_3)_2(CO)_2$(Me-DAB), model system for the $Ru(SnPh_3)_2(CO)_2$(α-diimine) complexes, the visible part of the absorption spectrum has been assigned in agreement with the available experimental data. A mechanism has been proposed for the photoinduced homolytic rupture of the Ru–Sn bond in this class of complexes. The shape of the potential energy curve associated with the low-lying ^{3}SBLCT state corresponding to the $\sigma 2 \rightarrow \pi^*_{Me-DAB}$) excitation confirms the pre-dissociative mechanism originating from this state. The bound character of the ^{1}SBLCT absorbing state excludes a fast direct decomposition of these molecules. The large ^{1}SBLCT–^{3}SBLCT energy gap explains the low emission quantum yield associated with the long emission lifetime originating in the ^{3}SBLCT state. The short-lived emission of higher energy can be attributed to the ^{1}SBLCT absorbing state itself. The small Stokes shifts observed in these molecules is confirmed by the relative position of the potential energy curves minima. The present work does not include spin–orbit effects (splitting of the triplet states and singlet–triplet interactions), which should be very important in the presence of three covalently bound heavy metal centres. The next step of the theoretical study will be the investigation of the excited states dynamics through wavepacket propagations on spin–orbit coupled potentials.

Acknowledgements

The authors are grateful to Professor D.J. Stufkens for helpful discussion and to Professor S. Zalis for the preliminary DFT results. This work has been undertaken as part of the European collaborative COST project (D14/0001/99). We thank the Departement de Chimie of the CNRS for specific COST financial support. M.T. thanks the Centre National des Œuvres Universitaires et Scolaires and the Tunisian government. The calculations have been carried out either at the IDRIS (Orsay, France) through a grant of computer time from the Conseil Scientifique or at the LCQS (Strasbourg, France).

References

[1] H.A. Nieuwenhuis, D.J. Stufkens, A. Oskam, Inorg. Chem. 33 (1994) 3212.
[2] H.A. Nieuwenhuis, D.J. Stufkens, A. Vlček Jr., Inorg. Chem. 34 (1995) 3879.
[3] H.A. Nieuwenhuis, D.J. Stufkens, R.A. McNicholl, A.H.R. Al-Obaidi, C.G. Coates, S.E.J. Bell, J.J. McGarvey, J. Westwell, M.W. George, J.J. Turner, J. Am. Chem. Soc. 117 (1995) 5579.
[4] H.A. Nieuwenhuis, M.C.E. Van de Ven, D.J. Stufkens, A. Oskam, K. Goubitz, Organometallics 14 (1995) 780.
[5] M.P. Aarnts, M.P. Wilms, K. Peelen, J. Fraanje, K. Goubitz, F. Hartl, D.J. Stufkens, E.J. Baerends, A. Vlček Jr., Inorg. Chem. 35 (1996) 5468.
[6] M.P. Aarnts, D.J. Stufkens, A. Vlček Jr., Inorg. Chim. Acta 266 (1997) 37.
[7] M.P. Aarnts, D.J. Stufkens, A. Oskam, J. Fraanje, K. Goubitz, Inorg. Chim. Acta 256 (1997) 93.
[8] M.P. Aarnts, F. Hartl, K. Peelen, D.J. Stufkens, C. Amatore, J.N. Verpeaux, Organometallics 16 (1997) 4686.
[9] M.P. Aarnts, M.P. Wilms, D.J. Stufkens, Organometallics 16 (1997) 2055.
[10] M.P. Aarnts, A. Oskam, D.J. Stufkens, J. Fraanje, K. Goubitz, N. Veldman, A.L. Spek, J. Organomet. Chem. 531 (1997) 191.
[11] D.J. Stufkens, M.P. Aarnts, J. Nijhoff, B.D. Rossenaar, A. Vlček Jr., Coord. Chem. Rev. 171 (1998) 93.
[12] D.J. Stufkens, A. Vlček Jr., Coord. Chem. Rev. 177 (1998) 127.
[13] S. Zalis, private communication.
[14] B.O. Roos, K. Andersson, M.P. Fülscher, L. Serrano-Andrès, K. Pierloot, M. Merchan, V. Molina, J. Mol. Struct. Theochem 388 (1996) 257.
[15] D. Andrae, U. Haeussermann, M. Dolg, H. Stoll, H. Preuss, Theor. Chim. Acta 77 (1990) 123.
[16] A. Bergner, M. Dolg, W. Kuechle, H. Stoll, H. Preuss, Mol. Phys. 80 (1993) 1431.
[17] K. Pierloot, B. Dumez, P.-O. Widmark, B.O. Roos, Theor. Chim. Acta 90 (1995) 87.
[18] K. Andersson, M.R.A. Blomberg, M.P. Fülscher, G. Karlström, R. Lindh, P.-Å. Malmqvist, P. Neogrady, J. Olsen, B.O. Roos, A.J. Sadlej, M. Schütz, L. Seijo, L. Serrano-Andrès, P.E.M. Sigbahn, P.-O. Widmark, Lund University, Sweden, 1997.
[19] M. Turki, C. Daniel, S. Zalis, A. Vlček Jr., J. Van Slageren, D.J. Stufkens, J. Am. Chem. Soc. submitted for publication.
[20] M. Turki, unpublished.
[21] M.C. Heitz, C. Ribbing, C. Daniel, J. Chem. Phys. 106 (1997) 1421.
[22] C. Daniel, D. Guillaumont, C. Ribbing, B. Minaev, J. Phys. Chem. A 103 (1999) 5766.